Biochemistry

 Volume 39, Number 24 June 20, 2000

Accelerated Publications

Does the Structure of the Water-Oxidizing Photosystem II−Manganese Complex at Room Temperature Differ from Its Low-Temperature Structure? A Comparative X-ray Absorption Study†

Carsten Meinke,‡ V. Armando Solé,§ Pavel Pospisil,‡ and Holger Dau*,‡,||

FB Biologie, Philipps-Universität Marburg, Lahnberge, D-35032 Marburg, Germany

Received October 19, 1999; Revised Manuscript Received April 3, 2000

ABSTRACT: Detailed information on room-temperature structure and oxidation state of the Photosystem II (PS II) manganese complex is needed to put mechanistic considerations on solid grounds. Because previously this information had not been available, the tetranuclear manganese complex was investigated by X-ray absorption spectroscopy (XAS) on PS II membrane particles at 290 K. Due to methodical progress (collection of XAS spectra within 10 s or less), significant X-ray radiation damage can be avoided; room-temperature XAS investigations on the PS II in its native membrane environment become feasible. Thus, the ambiguity with respect to the mechanistic relevance of low-temperature XAS results is avoidable. At 290 K as well as at 18 K, the manganese complex in its dark-stable state (S_1-state) seemingly is a Mn-$(III)_2Mn(IV)_2$ complex comprising two di-μ_2-oxo bridged binuclear manganese units characterized by the same Mn−Mn distance of 2.71−2.72 Å at both temperatures. Most likely, manganese oxidation states and the protonation state of the bridging oxides are fully temperature independent. Remarkably, at room-temperature manganese-ligand distances of 3.10 and 3.65 Å are clearly discernible in the EXAFS spectra. The type of bridging assumed to result in Mn−Mn or Mn−Ca distances around 3.1 Å is, possibly, temperature-dependent as suggested by distance lengthening upon cooling by 0.13 Å. However, mechanistic proposals on photosynthetic water oxidation, which involve the dimer-of-dimers model [Yachandra, V. K., et al. (1993) *Science 260*, 675−679] are not invalidated by the presented results.

In oxygenic photosynthesis, formation of dioxygen through water oxidation takes place at a tetranuclear manganese complex bound to the core proteins of the Photosystem II (PS II),[1] a pigment−protein complex embedded in the thylakoid membrane of plants and cyanobacteria. The release of the "byproduct" dioxygen has resulted in the oxygen-rich atmosphere presently encountered on Earth. For the photo-

† This research was supported by the German Bundesministerium für Bildung und Forschung (program Erforschung kondensierter Materie, Verbund 48). P.P. received financial support in form of a fellowship of the Alexander von Humboldt-Stiftung.

* To whom correspondence should be addressed. Phone: +49-(0)-30-838-53581. Fax: +49-(0)30-838-56299. E-mail: Holger.Dau@physik.fu-berlin.de.

‡ FB Biologie, Philipps-Universität Marburg, Lahnberge, D-35032 Marburg, Germany.

§ ESRF, BP. 220, 38043 Grenoble cedex, France.

|| Current address: FB Physik, Freie University Berlin, Arnimallee 14, D-14195 Berlin, Germany.

[1] Abbreviations: Chl, chlorophyll; EPR, electron paramagnetic resonance; EXAFS, extended X-ray absorption fine structure; OEC, oxygen-evolving complex; PS, photosystem; XAS, X-ray absorption spectroscopy.

10.1021/bi9924258 CCC: $19.00
Published on Web 05/26/2000

synthetic organism, more important, by the intricate redox chemistry of the manganese complex, water becomes accessible as a substrate for the photosynthesis of sugars and starch (*1*−*9*). Despite of considerable efforts and significant progress, mechanistically photosynthetic water oxidation is not adequately understood. Any sufficiently detailed mechanistic proposal needs to involve atomic-resolution models on the structure of the PS II manganese complex. Therefore, relevant structural information on the complex in its dark-stable state (S_1-state) and for other intermediate states of its functional cycle is of prime importance.

The active-site manganese complex seems to comprise four high-valent manganese ions, one calcium ion, one chloride, amino acid-derived ligands, oxides, or hydroxides bridging between manganese ions and water-derived ligands terminally coordinated to manganese (*1*−*9*). Mainly on the basis of results obtained by X-ray absorption spectroscopy (XAS) and guided by insights obtained through analysis of model compounds, a structural model of the PS II manganese complex has been proposed (*10*, *11*). According to this proposal, in the S_1-state there is a tetranuclear $Mn(III)_2Mn(IV)_2$ complex consisting of two di-μ_2-oxo-bridged "manganese dimers". These two binuclear units are assumed to be interconnected by a single mono-μ_2-oxo, bis-μ_2-carboxylato bridge resulting in a distance of about 3.3 Å between manganese ions. Furthermore, evidence has been presented that calcium is connected to manganese by bridging oxides resulting in a manganese calcium distance of 3.3−3.5 Å (*12*, *13*). However, in ref *14*, no evidence for the presence of a calcium ion close to manganese was found, and it has been proposed (*15*, *16*) that the Mn−Ca distance is close to 3.7 Å. The dimer-of-dimers model has gained considerable attention and has already entered student textbooks (*17*). This model is frequently employed for the interpretation of spectroscopic data (e.g., in ref *18*), for setting up quantum chemical calculations (e.g., in ref *19*), as a "target structure" for synthetic models (e.g., in ref *20*) and for formulation of detailed mechanistic models on photosynthetic water oxidation (*4*, *19*, *21*−*24*).

It often escaped attention that the dimer-of-dimers model is based on XAS (mainly) and EPR data (to a lesser extent) collected at low temperatures (usually either around 80 K or below 20 K), whereas the large body of kinetic data has been collected, necessarily, at temperatures which allow photosynthetic water oxidation to proceed. [In this context noteworthily, the above-mentioned 3.3 Å distance has been observed only by EXAFS spectroscopy at temperatures below 20 K; at 80 K a distance of about 3.7 Å was found (*15*).] It should be mentioned that already in 1981 a pioneering XAS investigation using so-called broken chloroplast was carried out at room-temperature by Melvin Klein and co-workers (*25*, *26*). Taking into consideration the methodical progress with respect to PS II preparations and X-ray absorption spectroscopy on protein-bound metal centers, it cannot surprise that in 1981, according to present standards, sufficiently detailed and unambiguous information on structure and oxidation state of the manganese complex at room temperature was not obtainable.

Taking into consideration insights obtained by decades of protein crystallography, the likelihood for large-scale structural rearrangements upon freezing appears to be relatively small. However, at cryogenic temperatures, the medium pH and local pH as well as pK_A values are essentially unknown and, presumably, mostly different from the respective room temperature values. Thus, the occurrence of temperature-dependent protonation states changes is rather more likely than improbable. With respect to the PS II manganese complex the certainly conceivable change from a μ-oxo to a μ-hydroxo bridge is of particular interest, because interpretation of spectroscopic data, advanced quantum chemical calculations, and formulation of detailed mechanistic models require knowledge on the protonation state of the bridging oxides. Another potentially temperature-dependent property is the manganese oxidation state. It has been proposed that redox equilibria are involved in photosynthetic water oxidation (see, e.g., ref *3*). The involvement of redox equilibria would imply temperature-dependent redox state changes (unless the enthalpic contributions to the free energy of the involved states matched exactly). In conclusion, the occurrence of relevant temperature-dependent changes of the PS II manganese complex needs to be considered seriously. Results on room-temperature structure and oxidation state of the manganese complex are required to put mechanistic considerations on solid grounds.

Whereas detection of EPR signals stemming from the PS II manganese complex seems to require the use of liquid-helium temperatures ($T < 20$ K), XAS on metalloproteins is not necessarily limited to measurements at low temperatures. However, the rate of so-called radiation damage caused by the X-ray irradiation is significantly accelerated at higher temperatures (see, e.g., ref *27*). Thus, room-temperature measurements on metalloproteins require particularly careful assessment of radiation-induced modifications of the investigated metal site, and subsequently, choice of an appropriate experimental strategy to avoid any significant influence of radiation effects on experimental results. At room temperature, X-ray irradiation may influence structure and metal oxidation state already within a few seconds. But as demonstrated in the following, optimized samples and rapid-scan capabilities of a modern synchrotron source render feasible XAS investigations on room-temperature structure and oxidation state of the oxygen-evolving PS II manganese complex.

EXPERIMENTAL PROCEDURES

PS II membrane particles and XAS-samples were prepared as described elsewhere (see ref *28*, oxygen-evolution activity of 1250−1400 μmol h^{-1}/mg of Chl). After controlled (partial) dehydration for 6 h, the Chl concentration of the obtained XAS samples had been 33 mg of Chl/g corresponding to a manganese concentration of approximately 17 ppm.

XAS measurements were carried out at the undulator beamline ID 26 of the European Synchrotron Radiation Facility (ESRF) in Grenoble (France) as described in the following; for further details, see refs *29*−*31*. Directly after passing the I_0-detector, the X-ray beam hit the sample surface. The beam profile was roughly Gaussian-shaped with horiziontal and vertical halfwidths of 0.2 and 0.8 mm, respectively. We estimate the photon flux at the sample to be approximately 0.5×10^{12} s^{-1}. X-ray fluorescence was detected perpendicular to the beam direction by a PIN photodiode (22 mm diameter, Eurisys Messures) positioned at approximately 4 cm distance of the sample's center. For

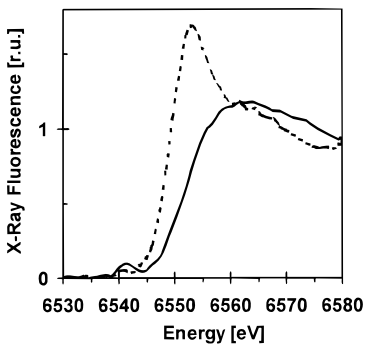

FIGURE 1: Room temperature spectra of the intact manganese complex (solid line) and the X-ray photoreduced complex (broken line). The displayed part of each spectrum has been collected within about 1 s. For the solid-line spectrum the X-ray exposure time amounts to approximately 1.5 s at the turning point of the edge. The dotted-line spectrum was collected subsequently to X-ray exposure for 150 s. Averaging of spectra was not employed.

suppression of scattered X-rays a filter consisting of chromium was mounted directly in front of the photodiode's active surface (6-absorption length filter, EXAFS Materials Inc.). To maximize the fluorescence signal, the open frontside of the sample-containing cavity (acrylic glass frame backed by a thin Kapton tape, inner dimensions of the frame $15 \times 2.5 \times 1$ mm^3) was exposed to the exciting X-ray beam, and the sample was mounted such that X-ray fluorescence reached the photodiode detector without passing any polymer foil. By moving the sample horizontally (and perpendicular to the beam direction) by 1 mm, several spots on the sample surface were exposed to X-rays and used for collection of spectra. We confirmed that spectra collected on a previously unused spot of the sample surface did not differ from spectra collected on a freshly mounted sample. For the sake of simplicity, in the following X-ray fluorescence excitation spectra of the PS II manganese complex are denoted as X-ray absorption spectra.

Spectra were collected by scanning of a Si 220 crystal monochromator cooled to −130 °C; efficient harmonic rejection was achieved by using two mirrors (Si and fused silica). For collection of X-ray edge spectra, the monochromator was scanned continuously with constant velocity (meaning approximately constant value of $\Delta E/\Delta t$), and the fluoresence signal was integrated over a time period of 20 ms. Depending on scanned energy range and scanning time period, the value of ΔE was either close to 1 eV (for the data shown in Figure 1) or smaller (0.5 and 0.2 eV, for various control experiments). Notewortily, we found that edge-position values (determined as described below) were independent of the scanning velocity ($\Delta E/\Delta t$) and of ΔE, the energy step width (holds for values of ΔE smaller than or equal to 1 eV). For the edge spectra shown in Figure 1 and referred to in Table 1, averaging of scans was not required because the achieved signal-to-noise ratio was sufficiently good for precise determination of values for the edge position (standard deviation of 0.05 eV, $n = 32$) by the "integral method" described elsewhere (*32*).

For collection of EXAFS spectra, monochromator and undulator gap were scanned simultaneously with essentially constant $\Delta E/\Delta t$, such that the monochromator energy permanently matched the undulator's peak energy. The total scanning period (for preedge background plus edge and EXAFS range) had been 10 s (scan range: 6500−7000 eV, $\Delta t = 20$ ms, $\Delta E \approx 1$ eV). About 12 EXAFS scans were averaged for each spectrum later subjected to curve fitting (spectra a, b, and c in Table 2).

For all scans on PS II preparations, X-rays passing through the sample were employed to record simultaneously the absorption spectrum of $KMnO_4$ powder on Kapton tape positioned in front of a photodiode detector. The X-ray energy found for the position of the $KMnO_4$ preedge peak (simulation of the peak using a Gaussian function plus quadratic background polynomial) was used for controlling and, if required, correcting the energy scale as described elsewhere (*28*). Typically, the position of the $KMnO_4$ preedge peak remained absolutely constant for several hours or even days, and recalibration of the energy scale was not required. By Gaussian fits the fwhm (full-width at half-maximum) of the preedge peak was determined to be 1.65 and 2.02 eV for ΔE of 0.2 and 1 eV (energy step per integration time period of 20 ms), respectively. We confirmed that this (anticipated) broadening of the $KMnO_4$ preedge peak observed for an increase in the energy stepwidth does not affect accuracy and precision of the determined edge-position values significantly (meaning by less than 0.1 eV). After subtraction of the preedge background, normalization of all spectra and extraction of EXAFS spectra was carried out as described elsewhere (*33*).

In Table 1, not only the X-ray edge position but also an estimate of the average manganese-oxidation state is provided. For this purpose, a value for the X-ray edge position (E_{edge}) was determined by the integral method described in ref *32*. Application of this integral method to the XAS spectra of manganese compounds containing exclusively oxygen ligands in the first coordination sphere (mainly manganese oxides) and comparison of the obtained E_{edge}-values to the respective formal manganese oxidation states (n_{ox}) yielded the following equation (see also ref *32*):

$$E_{edge} \approx 6539.6 \text{ eV} + 3.5 \text{ eV} \times n_{ox} \qquad (1)$$

The n_{ox}-values presented in Table 1 are calculated by means of eq 1 using the respective E_{edge} values. The n_{ox}-values are presented to illustrate the advancement of X-ray photoreduction by providing an estimate of the mean manganese oxidation state. We do not claim that eq 1 is of universal validity for manganese compounds; analysis of a more extended collection of manganese compounds might result in modifications of eq 1.

Low-temperature spectra used for comparison were collected at the XAS beamline of the Hamburg outstation of the EMBL (European Molecular Biology Laboratory) at approximately 18 K as described in ref *33* using "conventional" experimental conditions for XAS on metalloenzymes [energy-resolving multi-element fluorescence detector, scanning periods of 15−30 min, increased scanning times for energies corresponding to high *k*-values, "magic-angle excitation" (*34*)]. The S_1-state spectrum is identical to the corresponding spectrum shown and discussed in Schiller et al. (*33*); S_2-state spectra were collected on samples driven to the S_2-state by a 200 K illumination protocol (*35*).

The 30 K S_1-state data of Table 2 was collected at the ESRF using a liquid helium cryostat, but using otherwise essentially the same experimental scheme employed for

Table 1: Edge Position and Estimated Manganese Oxidation State for Various X-ray Exposure Times

t (s)	1.5	4.5	7.5	10.5	13.5	150	1000
E_{edge} (eV)	6551.73	6551.73	6551.54	6551.41	6551.18	6547.46	6547.04
n_{ox}	3.47	3.47	3.41	3.38	3.31	2.25	2.13
Δn_{ox}		0.00	0.06	0.09	0.16	1.22	1.34

Table 2: Simulation Results of k^3-Weighted EXAFS-Spectra of the PS II−Manganese Complex for Room Temperature and 20 K Spectra

	(Ia) O			(Ib) O			(II) Mn			(III) Mn			(IV) O			
	N	R (Å)	$2\sigma^2$ (Å^2)	N	R (Å)	$2\sigma^2$ (Å^2)	N	R (Å)	$2\sigma^2$ (Å^2)	N	R (Å)	$2\sigma^2$ (Å^2)	N	R (Å)	$2\sigma^2$ (Å^2)	RF (%)
(a) 290 K[a]	4.90	1.862	0.030	0.60	2.203	0.002[f]	1.01	2.715	0.010	0.75[f]	3.062	0.022	3.5[f]	3.642	0.006	5.2
(b) 290 K[a]	5.03	1.861	0.032	0.47	2.217	0.002[f]	1.03	2.713	0.011	0.75[f]	3.103	0.015	3.5[f]	3.660	0.006	6.9
(c) 290 K[a]	4.73	1.866	0.030	0.77	2.223	0.002[f]	0.92	2.711	0.011	0.75[f]	3.138	0.017	3.5[f]	3.649	0.007	1.3
290 K, avg[b]	4.88	1.863	0.030	0.62	2.214	0.002[f]	0.98	2.713	0.011	0.75[f]	3.101	0.018	3.5[f]	3.650	0.006	4.5
(±)[c]	0.12	0.002	0.001	0.12	0.009		0.05	0.002	0.001		0.031	0.003		0.007	0.000	
18 K, S1[d]	4.46	1.855	0.016	1.04	2.047	0.002[f]	1.14	2.717	0.003	0.75[f]	3.231	0.013	3.5[f]	3.558	0.026	15
18 K, S2[d]	5.05	1.856	0.016	0.45	2.058	0.002[f]	1.01	2.715	0.004	0.75[f]	3.268	0.018	3.5[f]	3.577	0.013	11
30 K, S1[e]	5.10	1.857	0.025	0.40	2.124	0.002[f]	0.96	2.706	0.002	0.75[f]	3.250	0.019	3.5[f]	3.569	0.019	8

[a] Spectra of dark-adapted PS II preparations collected at room temperature. [b] Mean values of results obtained for spectra a, b, and c. [c] Standard deviation. [d] Results obtained by measurements at 18 K for S_1-state and S_2-state samples (slow-scanning, energy-resolving fluorescence detector). [e] Results obtained by measurements at 30 K for the S_1-state (rapid-scanning, photodiode plus chromium filter for fluorescence detection). [f] Fixed values (see text).

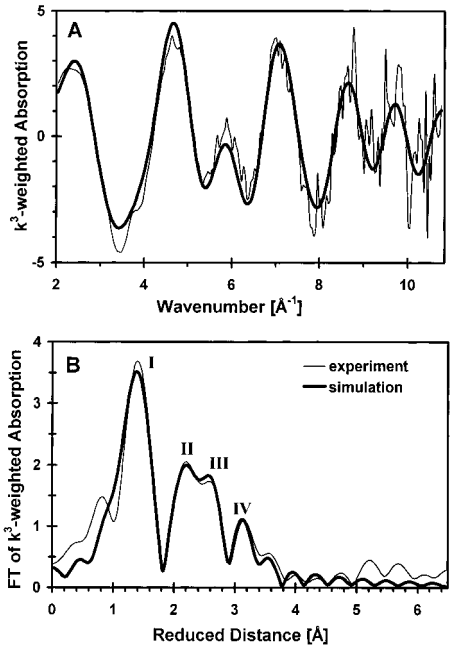

FIGURE 2: EXAFS spectra of the PS II manganese complex at 290 K. (A) k^3-weighted spectra. (B) Fourier transforms. Experimental (thin line) and simulated spectra as obtained by curve-fitting (thick line) are shown for spectrum b of Table 2. To carry-out least-squares fits, the unfiltered k-spectra shown in panel A were considered for k-values ranging from 2.8 to 10.8 Å^{-1} (or 6582 to 7000 eV); using the thus obtained fit parameters, the simulated spectrum has been calculated for a more extended k-range starting at 2.0 Å^{-1}.

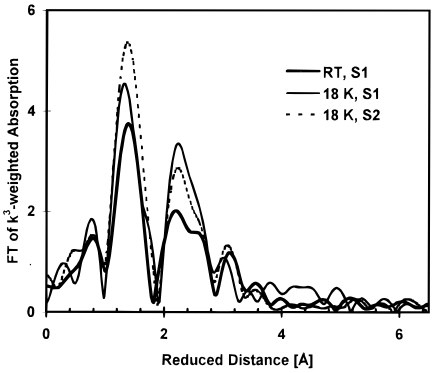

FIGURE 3: Fourier transformed EXAFS spectra collected at room temperature (thick solid line) and at 18 K (thin solid line, S_1-state; broken line, S_2-state). The shown Fourier transforms of low-temperature spectra for the PS II manganese complex in its S_1- and S_2-state differ from Fourier transforms which have been presented by the group of Klein, Sauer, and Yachandra (10−13) because different parameters were chosen for calculation of Fourier transformed spectra (see Materials and Methods); presumably, there is no major difference in the data itself.

collection of room-temperature spectra (fluorescence detection by photodiode plus chromium filter, scanning period of 8 s, Δt of 10 ms). Because the rate of X-ray photoreduction of the manganese complex was found to be significantly slower at 30 K, four scans per sample positions were used for data evaluation; 45 scans were averaged for the spectrum referred to in Table 2.

The parameters for conversion to k^3-weighted k-space data had been $E_0 = 6540$ eV, 200 data points equidistant in k. For the Fourier transforms shown in Figures 2 and 3, we used $E_0 = 6546$ eV (equal to the value used for simulation of EXAFS spectra), data points ranging from 15 to 450 eV above E_0, fractional cosine window (10% of k-range at low-k and high-k side of the spectrum).

The simulation results presented in Table 1 were obtained as described in the following. All parameters labeled by footnote *f* have been fixed to reasonable values during the fit to avoid an inacceptable number of free parameters. Assuming a mixture of five-coordinated and six-coordinated manganese, the sum of N_{IA} and N_{IB} was required to be 5.5. Phase functions were calculated using FEFF (see ref *36*, version FEFF7); curve-fitting of k^3-weighted k-spectra was carried out on a Pentium personal computer using the windows software XSIM of Jens Dittmer (Marburg). The EXAFS amplitude reduction factor was selected to be 0.85; for all backscattering shells the used energy treshold (E_0) was 6546 eV, a value which had been found to be appropriate by simulation of numerous manganese X-ray absorption spectra. This value of the invariable E_0 is close to the (invariable) value of 6545 eV used by Penner-Hahn and co-

workers (*14*). For carrying out least-squares fits, the error sum was calculated for k^3-weighted *k*-spectra for *k*-values corresponding to energies ranging from 6582 to 7000 eV. [It is noteworthy that the fit range traditionally used by Klein and co-workers (*11*−*13*, *44*, *45*) starts at higher energies, whereas others are using fit-range boundaries similarly low as 6582 eV or even lower (*14*−*16*, *33*). Today it is mostly believed that progress in EXAFS theory allows successful simulations also close to the absorption edge. It is conceivable that multiple-scattering contributions, which are not considered in the presently used fit approach, are particularly pronounced close the X-ray edge. However, due to the orthogonality of sine functions, the high *R* contributions to the EXAFS spectra stemming from multiple scattering do not interfere significantly with the curve-fitting of the low *R* single-scattering contributions related to absorber-backscatter distances below 3 Å. For distances above 3 Å, multiple scattering contributions might be of relevance, but not only in the energy range close to the absorption edge.]

In the last row of Table 2, a measure for the error is presented which is referred to as the filtered *R*-factor or "RF". The RF value was obtained by calculation of the standard EXAFS *R*-factor for experimental and simulated data previously "filtered" by Fourier-isolation using a rectangular window ranging from 1.3 to 3.6 Å. In contrast to the unfiltered *R*-value, RF does neither depend on the fit quality outside of the considered *R*-range nor on the number of *k*-space data points chosen during the transition from energy to wavevector scale. It should be noted that Fourier-filtering was employed only for calculation of the RF-value (after curve-fitting); for curve-fitting itself exclusively unfiltered *k*-spectra had been used.

RESULTS AND DISCUSSION

Assessment of Radiation Damage. Due to absorption of X-ray photons by the atoms of the proteins, lipids and solvent molecules numerous radicals are formed (*27*, *37*) (presumably clearly more than 10 per X-ray photon; see ref *37*). Protein-bound transition metals in higher oxidation states become reduced due to electron transfer from a radiation-induced nearby anion radical. Reduction of the metal ion typically results in a shift of the X-ray edge position to lower energies, which often is accompanied by changes in the edge shape. Therefore, analysis of edge spectra can facilitate an assessment of the radiation influence on the metal site.

The fluorescence-detected X-ray absorption edge spectrum of the undamaged PS II manganese complex in its dark-state and spectrum of the same sample collected after 150 s of X-ray exposure are shown in Figure 1; even longer X-ray exposure time result in essentially no further changes (not shown). The edge-position and the shape of the spectrum (in particular, the peak around 6552 eV) collected after 150 s X-ray are highly characteristic of manganese in the oxidation state +2. Seemingly, prolonged X-ray exposure results in complete conversion of high-valent manganese ions to Mn(II).

It is, in the present context, of particular interest to determine the maximally acceptable irradiation time. For this purpose, X-ray edge spectra were analyzed using the recently proposed "integral method" for determination of edge-positions as well as the relation between edge position and manganese oxidation state (*32*). Considering X-ray photoreduction of 7.5% of all manganese ions (by one oxidation equivalent) to be acceptable, the results presented in Table 1 suggest that the maximal irradiation for the PS II manganese complex at room temperature is, for the used experimental conditions, about 10 s. Consequently, the room-temperature EXAFS spectra discussed in the following were collected using an irradiation period of 10 s. (The chosen limit of 7.5% may appear to be rather stringent. However, reduction of 7.5% of all manganese ions might correspond to reduction of 30% of the tetra-manganese complexes.)

Mn Oxidation State at Room Temperature. The results shown in Table 1 suggest that the mean manganese oxidation state at room temperature is 3.5. The edge position is essentially identical to the value we determined at 18 K (*28*); features in the edge shape characteristic of Mn(II) are not observed (in the absence of X-ray photoreduction). Thus we conclude that, most likely, a $Mn(III)_2-Mn(IV)_2$ complex is present at low temperatures as well as at room temperature. (For a discussion of edge positions and its relation to oxidation states, see refs. *6*, *9*, *28* and *32*.)

Room-Temperature EXAFS Spectra. The k^3-weighted EXAFS spectra shown in Figure 2 are similar, but not fully identical, to low-temperature spectra of the PS II manganese complex in its S_1-state (for comparison see, e.g., ref *33*). The Fourier transformed spectra exhibit three major peaks with a clearly resolved shoulder at the long-distance side of peak II. Each peak is related to backscattering atoms at a distances to the X-ray absorbing manganese ion which equals the indicated reduced distance plus about 0.5 Å. Thus, already the visual inspection of the Fourier transforms suggests backscattering atoms to be at about 1.9 Å (I), 2.7 Å (II), 3.1 Å (III), and 3.65 Å (IV). For a more detailed analysis, k^3-weighted spectra were subjected to curve-fitting. To facilitate the comparison of low-temperature versus room-temperature structure of the PS II manganese complex, EXAFS spectra (Figure 3) and fit results (Table 2) obtained for EXAFS data collected at 18 and 30 K are also presented and discussed in the following.

First Coordination Sphere. In the S_1-state, the oxygen-evolving complex is, most likely, a $Mn(III)_2-Mn(IV)_2$ complex as discussed above, and the manganese ions are presumably five- or six-coordinated predominantly to oxide ligands. For the presented EXAFS simulations we assumed that, on the average, 5.5 oxygen atoms are coordinated to the manganese ions. For the room-temperature EXAFS data, only if a second shell of backscattering atoms with absorber-backscatterer distances around 2.2 Å is considered explicitly, a good fit is obtained. (To keep the number of free parameters sufficiently low, the Debeye-Waller parameter of this sub shell was fixed to a value which allows for high-quality simulations. Other values, however, did not necessarily result in significantly higher error sums.) These backscattering atoms might be related to terminally coordinated water, to nitrogen ligands, or even chloride ligated to manganese. Also, it cannot be excluded fully that ligands to a small amount of adventitious Mn^{2+} are involved. In any event, at room temperature, the EXAFS stemming from the major fraction of first sphere ligands is describable by a Gaussian distribution function with a half-width of about 0.14 Å (half-width at half-maximum: $\Delta R^2 = 2\,\sigma^2 \ln 2$) centered at 1.86 Å.

For the S_1-state spectra collected at 18 K, a shoulder is visible at the first Fourier-peak which is related to backscattering atoms around 1.95 Å as discussed in Schiller et al. (*33*). Therefore, the two-shell fit approach used here is not fully adequate for this low-temperature data. Consequently, the corresponding RF value in Table 2 is relatively high, and the low-temperature value for the Ib-distance is questionable. Presumably the 1.95 Å distance is not resolvable at room temperature because of an increased dynamic disorder due to thermally excited vibrations.

Mn−Mn Distance of 2.7 Å. The 2.7 Å EXAFS interaction, which is the best resolved and least ambiguous one, is commonly assigned to backscattering by manganese (*15*, *38*, *39*). At room temperature as well as at low temperatures, N_{II} equals 1.0 (±0.1), indicating the presence of two pairs of manganese ions at a mean distance of 2.71−2.72 Å, a distance which is characteristic of di-μ_2-oxo-bridged manganese pairs (*40*, *41*). A high similarity between room temperature and low-temperature structure of these di-μ-oxo-bridged manganese pairs is suggested by the striking numerical identity of the values for the Mn−Mn distance. The only observed difference is an increased σ_{II}, the Debye−Waller parameter, at room temperature, a finding which is explainable by an increased "dynamic disorder" (or "dynamic distance spread") due to thermal excitation of vibrational modes.

Ligands at Distances Greater Than 2.9 Å. Two shells of backscattering atoms with mean distances to the absorbing manganese ions of about 3.1 and 3.65 Å are clearly resolvable by curve-fitting (as already suggested by the Fourier transforms shown in Figure 2). However, with respect to these relatively weak, long-distance EXAFS interactions, it is of importance to keep in mind the limitations of the method. It has been not possible to determine unambiguously to what extent the individual backscatterer shells are related to backscattering by heavy atoms (Mn, Ca) or lighter atoms (O, N, C). Particularly good fits were achieved assuming that the 3.1 Å interaction is dominated by heavy backscatterers (use of backscattering amplitudes calculated for manganese), whereas the 3.6 Å interaction is dominated by lighter atoms (backscattering amplitudes calculated for oxygen). Furthermore, to decrease the correlation between fit parameters it was necessary to fix the coordination number to values which, on one hand, result in high-quality fits and, on the other hand, are chemically reasonable. The chosen value of N_{III} (=0.75) is consistent with one Mn−Mn interaction per tetranuclear complex ($N = 0.5$) plus one Mn−Ca interaction ($N = 0.25$). However, values of N_{III} ranging from 0.5 to 1.5 also result in acceptable fits. Tentatively, we conclude that existence of a Mn−Mn distance around 3.1 Å is relatively likely, but certainly not unambiguously indicated by the data. No conclusion is possible with respect to the question whether and to what extent backscattering by calcium contributes.

Assuming that the PS II manganese complex consists of two dimers of di-μ-oxo-bridged manganese ions, one has to anticipate EXAFS oscillations due to backscattering by the oxygen ligands in cis position to the bridging oxides. This third-coordination sphere EXAFS is likely to contribute significantly to the experimentally observed 3.6 Å-EXAFS oscillations. Other contributions (e.g., backscattering by Ca at 3.7 Å as proposed in refs *15* and *16*), however, cannot be excluded. Furthermore, at 3.6 Å an influence of multiple scattering to the EXAFS oscillations is imaginable (but presumably of minor importance, see ref *42*).

Room-Temperature versus Low-Temperature Structure. The unchanged 2.7 Å EXAFS interaction is highly suggestive that at room temperature as well as at liquid helium temperatures two pairs of Mn ions are connected by di-μ-oxo bridges. The observation of fully unchanged distances implies that the bridging mode is temperature independent with respect to the protonation state of the bridging oxides, which are, most likely, fully unprotonated at both temperatures (protonation of a single oxide of a di-μ-oxo bridge results in a Mn−Mn distance of about 2.81, see ref *43*). It is likely that the change in temperature from 295 to 18 K causes significant pH changes; a decrease in the pH by several units is imaginable. Seemingly the p*K* of the bridging oxides is low enough to ensure a fully unprotonated state at all temperatures. Furthermore, distance changes which are indicative for temperature-induced structural changes involving additional bridging ligands are not observed (e.g., formation or dissolution of a μ-carboxylato bridges between the di-μ-oxo-bridged manganese ions should result in a change of the corresponding 2.7 Å distance by about 0.05 Å).

The lengthening of the 3.1 Å distance (at room temperature) to 3.25 Å (at 18 K) points toward structural changes. Mn−Mn distances ranging from 3.1 to 3.5 Å can result from manganese ions connected by either μ_2-oxo or μ_2-hydroxo bridges supported by μ_2-carboxylato bridges (*40*, *41*). Assuming there is a mono-μ_2-oxo, bis-μ_2-carboxylato bridge at room temperature, the distance lengthening upon lowering the temperature could be related to protonation of the bridging oxides or due to dissolution of one carboxylato bridge. Thus, the observed distance change could be indicative of structural changes which involve breaking and formation of covalent bonds. Presently, however, alternative explanations cannot be excluded. For example, anharmonicity of the thermally excited vibrations might result in a mean distance which is different from the low-temperature equilibrium distance. Also, a complex superposition of EXAFS oscillations (perhaps) stemming from various types of backscattering atoms (Mn, Ca, O, N, C, and Cl) might result in spectral changes which mimic modifications of the equilibrium structure due to convoluted temperature-dependent changes of the various Debye−Waller factors.

The Debye−Waller factor of the 3.6 Å distance is significantly enlarged upon freezing. Due to the above-mentioned methodical limitations, this observation does not necessarily indicate an increased static disorder at low temperatures. Equally likely appears to be a relation to the structural changes which cause the lengthening of the 3.1 Å distance.

In summary, the dimer-of-dimers model (as proposed in refs *10* and *11* and supported by, e.g., refs *44* and *45*) can account for the EXAFS-data collected below 20 K and at room temperature. The protonation state of the di-μ_2-oxo-bridges is temperature independent. The type of bridging between manganese ions (or between manganese and calcium) resulting in internuclear distances around 3.2 Å is, possibly, temperature dependent. As far as the S_1-state is concerned, mechanistic models of photosynthetic water oxidation which involve the dimer-of-dimers model are not

invalidated by the presented results on the structure of the PS II manganese complex at room temperature.

Perspectives. By this work it has been demonstrated, for the first time, that high-quality room-temperature XAS investigations on PS II particles are feasible if an appropriate experimental strategy is used. The increase of Debye−Waller factors upon temperature increase results in more damped EXAFS-oscillations, but the amount of extractable structural information is found to be not significantly lower at room temperature. (On the contrary, two shells of backscattering atoms at distances greater than 2.9 Å are clearly resolvable at room temperature, whereas at 18 K the existence of two resolvable backscatterer shells is debatable.) Room-temperature XAS investigations open a new road to gain insights in the structure−function relationships involved in photosynthetic water oxidation. Structural investigations under defined (e.g., with respect to pH) and "almost native" conditions become viable; the ambiguity with respect to the relevance of low-temperature results is avoidable. In the future, time-resolved XAS investigations, which require experiments at or close to room temperature, may provide further insights in the mechanism of photosynthetic water oxidation.

ACKNOWLEDGMENT

We are grateful to Drs. L. Iuzzolino, J. Dittmer, H. Schiller, W. Dörner (all Marburg), W. Meyer-Klaucke, and H. Nolting (both Hamburg) who prepared excellent samples (L. Iuzzolino) and collected data for the low-temperature spectra shown for comparison. We acknowledge the competent work of the technicians S. Feite, J. C. Collet-Fenetrier, and L. Leclerc (ESRF, Grenoble) and of the mechanics workshop at the FB Biologie (University Marburg). We thank Drs. A. Batschauer, D. Dörnemann, Kadenbach, H. Senger, R. Schulz, C. Elschenbroich, and O. Burghaus (all Marburg) and the members of the Graduiertenkolleg "Enzymchemie" (Marburg) for supporting this work in various ways. We are grateful to the Alexander von Humboldt-Stiftung for supporting Pavel Pospisil by generously providing a fellowship. We also acknowledge the fruitful methodical cooperation with the research groups of the Verbund 48 (EXAFS and XANES Untersuchungen mit Synchrotronstrahlung zur Struktur und Funktion biologisch wichtiger Metallzentren) in the program "Erforschung kondensierter Materie" of the German BMBF.

REFERENCES

1. Rutherford, A. W., Zimmermann, J.-L., and Boussac, A. (1992) in *The Photosystems: Structure, Function and Molecular Biology* (Barber, J., Ed.) pp 179−229, Elsevier, Amsterdam, The Netherlands.
2. Debus, R. J. (1992) *Biochim. Biophys. Acta 1102*, 269−352. Sauer, K., Yachandra, V. K., Britt, R. D., and Klein, M. P. (1992) in *Manganese Redox Enzymes* (Pecoraro, V. L., Ed.) pp 141−175, VCH, Weinheim, Germany.
3. Renger, G. (1993) *Photosynth. Res. 38*, 229−247.
4. Riggs-Gelasco, P. J., Mei, R., and Penner-Hahn, J. E. (1995) *Adv. Chem. Ser. 246*, 219−248.
5. Britt, R. D. (1996) in *Oxygenic Photosynthesis: The Light Reactions* (Ort, D. R., and Yocum, C. F., Eds.) pp 137−164, Kluwer Academic Publishers, Dordrecht, The Netherlands.
6. Yachandra, V. K., Sauer, K., and Klein, M. P. (1996) *Chem. Rev. 96*, 2927−2950.
7. Haumann, M., and Junge, W. (1996) in *Oxygenic Photosynthesis: The Light Reactions* (Ort, D. R., and Yocum, C. F., Eds.) pp 165−192, Kluwer Academic Publishers, Dordrecht, The Netherlands.
8. Rüttinger, W., and Dismukes, G. C. (1997) *Chem. Rev. 97*, 1−24.
9. Penner-Hahn, J. E. (1998) in *Metal sites in proteins and models. Redox centres.* (Hill, H. A. O., Sadler, P. J., and Thomson, A. J., Eds.) pp 1−33, Springer-Verlag, Heidelberg, Germany.
10. Sauer, K., Yachandra, V. K., Britt, R. D., and Klein, M. P. (1992) in *Manganese Redox Enzymes* (Pecoraro, V. L., Ed.) pp 141−175, VCH, Weinheim, Germany.
11. Yachandra, V. K., DeRose, V. J., Latimer, M. J., Mukerji, I., Sauer, K., and Klein, M. P. (1993) *Science 260*, 675−679
12. Latimer, M. J., DeRose, V. J., Mukerji, I., Yachandra, V. K., Sauer, K., and Klein, M. P. (1995) *Biochemistry 34*, 10898−10909.
13. Cinco, R. M., Roblee, J. H., Rompel, A., Fernandez, C., Yachandra, V. K., Sauer, K., and Klein, M. P. (1998) *J. Phys. Chem. B 102*, 8248−8256.
14. Riggs-Gelasco, P. J., Mei, R., Ghanotakis, D. F., Yocum, C. F., and Penner-Hahn, J. E. (1996) *J. Am. Chem. Soc. 118*, 2400−2410.
15. MacLachlan, D. J., Hallahan, B. J., Ruffle, S. V., Nugent, J. H. A., Evans, M. C. W., Strange, R. W., and Hasnain, S. S. (1992) *Biochem. J. 285*, 596−576.
16. MacLachlan, D. J., Nugent, J. H. A., Bratt, P. J., and Evans, M. C. W. (1994) *Biochim. Biophys. Acta 1186*, 186−200.
17. Shriver, D. F., Atkins, P. W., and Langford, C. H. (1994) in *Anorganic Chemistry*, Oxford University Press, Oxford, U.K.
18. Hasegawa, K., Ono, T., Inoue, Y., and Kusunoki, M. (1999) *Chem. Phys. Lett. 300*, 9−19.
19. Siegbahn, P. E. M., and Crabtree, R. H. (1999) *J. Am. Chem. Soc. 121*, 117.
20. Armstrong, W. H. (1992) in *Manganese Redox Enzymes* (Pecoraro, V. L., Ed.) pp 261−286, VCH, Weinheim, Germany
21. Pecoraro, V. L. (1992) in *Manganese Redox Enzymes* (Pecoraro, V. L., Ed.) pp 197−231, VCH, Weinheim, Germany.
22. Hoganson, C. W., and Babcock, G. T. (1997) *Science 277*, 1953−1956.
23. Szalai, V. A., Stone, D. A. and Brudvig, G. W. (1998) in *Photosynthesis: Mechanism and Effects* (Garab, G., Ed.) Vol. II, pp 1403−1406, Kluwer Academic Publishers, Dordrecht.
24. Pecoraro, V. L., Baldwin, M. J., Caudle, M. T., Hsieh, W.-Y., and Law, N. A. (1998) *Pure Appl. Chem. 70*, 925−929.
25. Kirby, J. A., Goodin, D. B., Wyrdrzynski, T., Robertson, A. S., and Klein, M. P. (1981) *J. Am. Chem. Soc. 103*, 5537−5542.
26. Kirby, J. A., Goodin, Robertson, A. S., Smith, J. P., Thompson, A. C., Cooper, S. R., and Klein, M. P. (1981) *J. Am. Chem. Soc. 103*, 5529−5537.
27. Peisach, J., Powers, L., Blumberg, W. E., and Chance, B. (1982) *Biophys. J. 38*, 277−285.
28. Iuzzolino, L., Dittmer, J., Dörner, W., Meyer-Klaucke, W., and Dau, H. (1998) *Biochemistry 37*, 17112−17119.
29. Gauthier, C., Solé, V. A., Signorato, R., Goulon, J., and Moguiline, E. J. (1999) *J. Synchrotron Rad. 6* 164−166.
30. Signorato, R., Solé, V. A., and Gauthier, C. (1999) *J. Synchrotron Rad. 6*, 176−178.
31. Solé, V. A., Gauthier, C. , Goulon, J., and Natali, F. (1999) *J. Synchrotron Rad. 6*, 174−175.
32. Dittmer, J., Iuzzolino, L.,, Dörner, W., Nolting, H.-F., Meyer-Klaucke, W., and Dau, H. (1998) In *Photosynthesis: Mechanism and Effects* (Garab, G., Ed.) Vol. II, pp 1339−1342, Kluwer Academic Publishers, Dordrecht.
33. Schiller, H., Dittmer, J., Iuzzolino, L., Dörner, W., Meyer-Klaucke, W., Sole, V. A., Nolting, H.-F., and Dau, H. (1998) *Biochemistry 37*, 7340−7350.
34. Dittmer, J., and Dau, H. (1998) *J. Phys. Chem. B 102*, 8196−8200.
35. Brudvig, G. W., Casey, J. L., and Sauer, K. (1983) *Biochim. Biophys. Acta 723*, 366−371.

36. Rehr, J. J., Mustre de Leon, J., Zabinsky, S. I., and Albers, R. C. (1991) *J. Am. Chem. Soc. 113*, 5135.
37. Dau, H., Dittmer, J., Iuzzolino, L., Schiller, H., Dörner, W., Heinze, I., Sole, V. A., and Nolting, H.-F. (1997) *J. Phys. IV France 7, C2*, 607−610.
38. Yachandra, V. K., Guiles, R. D., McDermott, A., Britt, R. D., Dexheimer, S. L., Sauer, K., and Klein, M. P. (1986) *Biochim. Biophys. Acta 850*, 324−332.
39. Penner-Hahn, J. E., Fronko, R. M., Pecoraro, V. L., Yocum, C. F., Betts, S. D., and Bowlby, N. R. (1990) *J. Am. Chem. Soc. 112*, 2549−2557.
40. Wieghardt, K. (1989) *Angew. Chem., Int. Ed. Engl. 28*, 1153−1172.
41. Larson, E. J., and Pecoraro, V. L. (1992) in *Manganese Redox Enzymes* (Pecoraro, V. L., Ed.) pp 1−28, VCH, Weinheim, Germany.
42. Dittmer, J., and Dau, H. (1996) *Ber. Bunsen-Ges. Phys. Chem. 100*, 1993−1998.
43. Larson, E. J., Riggs, J. E., Penner-Hahn, J. E., and Pecoraro, V. L. (1992) *J. Chem. Soc., Commun.* 102−103
44. DeRose, V. J., Mukerji, I., Latimer, M. J., Yachandra, V. K., Sauer, K., and Klein, M. P. (1994) *J. Am. Chem. Soc. 116*, 5239−5249.
45. Dau, H., Andrews, J. C., Roelofs, T. A., Latimer, M. J., Liang, W., Yachandra, V. K., Sauer, K., and Klein, M. P. (1995) *Biochemistry 34*, 5274−5287.

BI9924258